A brief update of angle-resolved photoemission spectroscopy on a correlated electron system



2009 J. Phys.: Condens. Matter 21 164217

(http://iopscience.iop.org/0953-8984/21/16/164217)

IOP Publishing Journal of Physics: Condensed Matter

J. Phys.: Condens. Matter **21** (2009) 164217 (7pp) doi:10.1088/0953-8984/21/16/164217

# A brief update of angle-resolved photoemission spectroscopy on a correlated electron system

**W S Lee, I M Vishik, D H Lu and Z-X Shen**

Department of Physics, Applied Physics, and Stanford Synchrotron Radiation Laboratory, Stanford University, Stanford, CA 94305, USA

Received 22 January 2009
Published 31 March 2009
Online at stacks.iop.org/JPhysCM/21/164217

**Abstract**

In this paper, we briefly summarize the capabilities of state-of-the-art angle-resolved photoemission spectroscopy (ARPES) in the field of experimental condensed matter physics. Due to the advancement of the detector technology and the high flux light sources, ARPES has become a powerful tool to study the low energy excitations of solids, especially those novel quantum materials in which many-body physics are at play. To benchmark today's state-of-the-art ARPES technique, we demonstrate that the precision of today's ARPES has advanced to a regime comparable to the bulk-sensitive de Haas–van Alphen (dHvA) measurements. Finally, as an example of new discoveries driven by the advancement of the ARPES technique, we summarize some of our recent ARPES measurements on underdoped high-$T_c$ superconducting cuprates, which have provided further insight into the complex pseudogap problem.

(Some figures in this article are in colour only in the electronic version)

The photoemission process, known more widely as the photoelectric effect, was first discovered by Hertz in 1887 [1]. Its microscopic mechanism was explained by Einstein using the revolutionary concept of 'light quanta' [2], which became a corner stone for the foundation of quantum mechanics. Along with the development of quantum mechanics, scientists started to realize that the photoemission process can be a powerful tool to study the electronic state of materials, which is fundamentally important in many fields, including chemistry, surface science, and condensed matter physics. The early valence band photoemission measurement on a solid state sample was performed by Berglund and Spicer in 1964 [3] on Cu and Ag. In this experiment, the edge of the valence band from the d orbital at 2 and 4 eV below the Fermi energy was resolved, which agrees with the predictions of the non-interacting band theory. Since then, the techniques of photoemission spectroscopy, especially angle-resolved photoemission (ARPES), have made significant progress and become one of the most crucial tools in studying the electronic properties of today's novel materials.

Angle-resolved photoemission spectroscopy records the number of photoelectrons at a given kinetic energy and emission angle with respect to the sample. By virtue of the energy and momentum conservation laws, one can then deduce the binding energy and the crystal momentum of the electron before it emitted away from the sample; therefore, momentum-dependent electronic structures of the sample can be resolved [4, 5]. This unique momentum-resolved ability makes ARPES a powerful tool for mapping the band structure and the Fermi surface topology. Furthermore, since the ARPES intensity is proportional to the single particle spectral function [4, 5], valuable information on the many-body effect can be revealed from spectral analysis. A typical set-up for a modern angle-resolved photoemission spectroscopy in a synchrotron radiation laboratory is shown in figure 1. The photons emitted from the undulator are guided toward a monochromator to produce the monochromatic photon beam at the desired excitation energy. The monochromatic beam is then focused and guided onto the sample to excite the photoelectrons. Finally, the photoelectrons are collected by the photoelectron analyzer. The whole system is under ultra-high vacuum with a pressure typically less than $5 \times 10^{-11}$ Torr to maintain the sample surface quality.

The recent development of the ARPES technique is heavily scientifically driven by the increasing demand to study quantum materials, represented by the cuprate

 

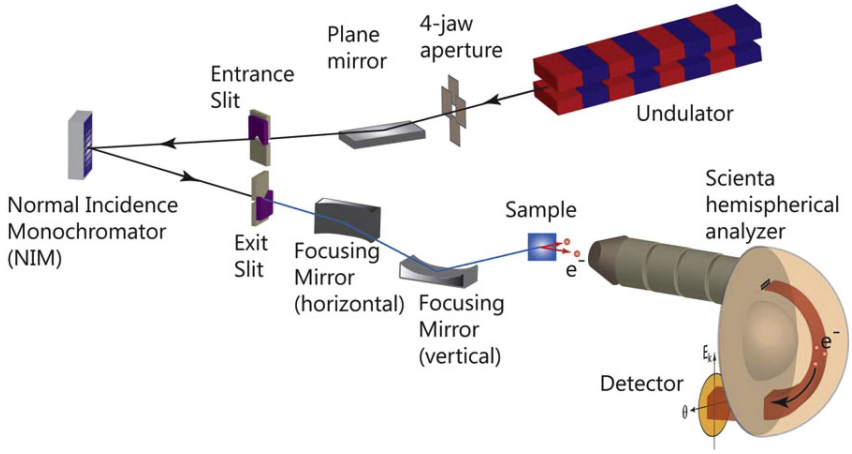


**Figure 1.** A sketch of a typical ARPES end station in a synchrotron radiation facility. The monochromator sketched here is the normal incident monochromator (NIM), which can generate high quality monochromatic light from 7 to 30 eV for ARPES measurements with less photon contamination from the higher order harmonic. The resolution of the experiment can be adjusted by changing the opening of exit slits and analyzer slit.

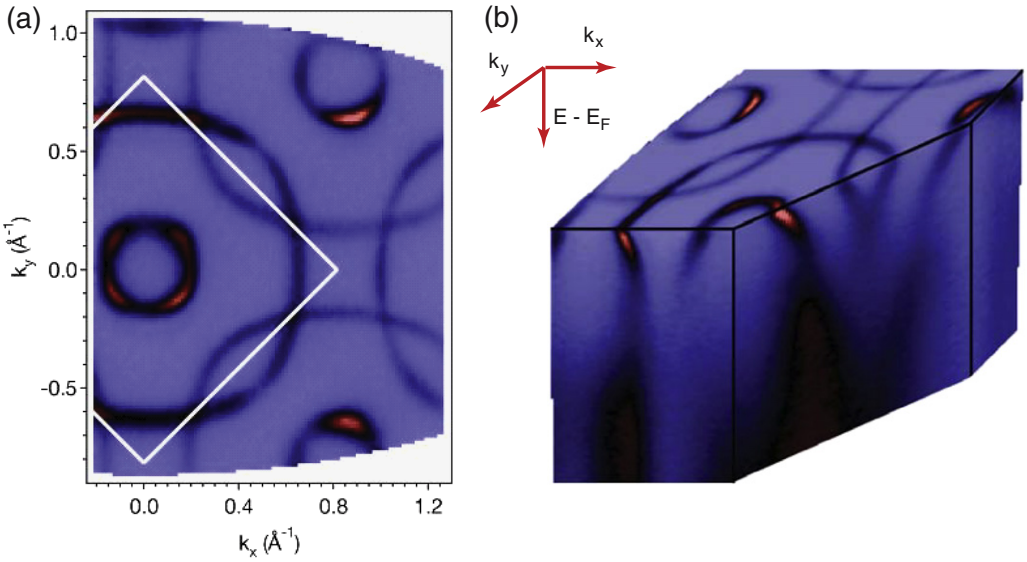


**Figure 2.** A set of ARPES data on $Sr_2RhO_4$ taken at an energy resolution of 8 meV. The Fermi surface (a) and the complete band structure mapping (b) are both shown. The total number of spectra is on the order of $10^4$, which were taken in 9 h of measurement time, corresponding to a data acquisition rate of ∼3 s per spectrum. Reproduced with permission from [8]. Copyright 2006 by The American Physical Society.

superconductors, and is tied closely to the technology development of both the photoelectron analyzer and the light sources. A major improvement of the detector technology is the advent of a two-dimensional image detecting method with a CCD. This imaging technology can record the energy spectrum along a cut line in the momentum space simultaneously, or a 2D image of a cut plane in the energy–momentum space. Compared to the older technology, which can only measure the energy spectra at one momentum point at one time, this 2D imaging method used by the current analyzer not only significantly increases the data collecting efficiency, but also greatly improves the momentum resolution, from 1° to ∼0.2°. On the other hand, ARPES measurements have benefited a lot from the maturing technology of the third generation synchrotron radiation facilities during the past decade, which can now routinely produce high flux ($>10^{12}$ photons $s^{-1}$) and narrow bandwidth (<10 meV) monochromatic photons. In addition, a high flux gas discharge lamp is also available, which has been used widely in laboratory-based ARPES systems. Equipped with 2D imaging detection techniques and the high flux light sources, a state-of-the-art ARPES system is capable of performing measurements at an energy resolution better than 10 meV with high efficiency (see figure 2 as an example).

Recently, ARPES measurements with ultra-high energy resolution better than 1 meV have been made possible by using a UV laser as the light source [6]. By using appropriate nonlinear crystals and frequency summing of the laser beam, one can produce VUV photons, which are suitable for ARPES measurements. So far, the highest photon energy that can be produced by this method is ∼7 eV, which is noticeably

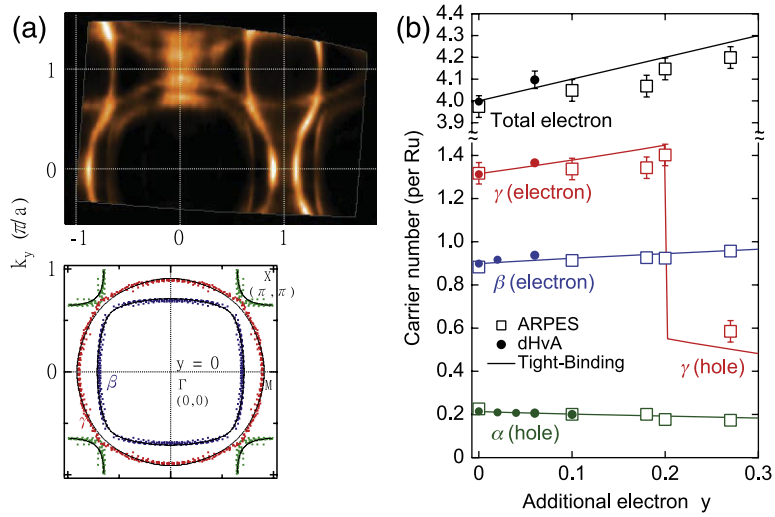


**Figure 3.** A benchmark of ARPES measurements on $Sr_{2-y}La_yRuO_4$. (a) The Fermi surface of the $Sr_{2-y}La_yRuO_4$ for $y = 0$. (b) dHvA (closed circles) and ARPES (open squares) data for the carrier number of each of the three Fermi surface sheets as a function of $y$. Reproduced with permission from [7]. Copyright 2007 by The American Physical Society.

lower than the regular photon energy normally used in a synchrotron light source. A benefit of performing ARPES measurements using low energy photons is a significant gain of the momentum resolution, since the conversion from the detector angle to the momentum space is proportional to the square root of the kinetic energy of the photoelectrons. In addition, the narrow bandwidth and high intensity of the laser beam make it possible to operate the photoelectron analyzer at an ultra-high resolution with high data acquisition efficiency. However, since the matrix element of ARPES spectra depends strongly on the excitation photon energy, the very limited photon energy tunability of the laser is a fundamental disadvantage of a laser-ARPES system. Clearly, the laser-ARPES system is a complement to the synchrotron-based ARPES system, but can hardly be a replacement.

For the rest of this article, we will demonstrate the capability of a state-of-the-art ARPES system by benchmarking with bulk-sensitive measurements. Finally, a scientific example of our recent gap measurements on high-$T_c$ superconducting copper oxides will also be summarized, in which new discoveries have been made by ARPES.

## 1. Benchmarking ARPES with bulk-sensitive measurements

Fermi surface (FS) topology is one of the most crucial properties determining the low energy excitations of an electronic system. The volume of the FS corresponds to the number of charger carriers available for low energy excitations; together with the effective mass of electrons at the Fermi level, the transport property of the system is mostly determined. The shape of the Fermi surface can be very important, too. It is known that instability toward a charge density wave or spin density wave formation can be induced if a finite portion of the Fermi surface can be connected by a constant wavevector, a situation called Fermi surface nesting. In principle, ARPES is an ideal tool for mapping the size and shape of the Fermi surfaces, since it measures the single particle spectrum directly. However, since the mean free path of the electron is very short inside a solid [5], ARPES measurement is extremely surface sensitive and its precision is generally expected to be lower than the classical FS probes based on de Haas–van Alphen (dHvA) or related effects. With the development of the ARPES technique, it would be important to benchmark the precision of ARPES measurement on materials whose FS can also be measured by bulk-sensitive measurement. Recent reports have demonstrated excellent agreements, as will be summarized in the following paragraph.

Figure 3 demonstrates the results of an ARPES measurement on doped ruthenates, $Sr_{2-y}La_yRuO_4$ [7]. The Fermi surfaces of these systems are rather complicated: as shown in (a), the Fermi surface topology consists of two electron pockets and one hole pocket; a rigid band shift due to different doping level $y$ is observed clearly through ARPES measurement. Figure 3(b) summarizes the number of charge carriers deduced from ARPES measurements, in good agreement with those measured by dHvA on $y = 0$ and 0.06. The charge carrier concentration for each pocket agrees very well between the values measured by ARPES and dHvA techniques, suggesting that today's ARPES technique is capable of measuring Fermi surface topology at a precision comparable to that measured by dHvA. An advantage of ARPES over the dHvA measurements, as also shown in figure 3(b), is that ARPES can measure the FS of the material with a wider range than the dHvA technique, because dHvA requires a long mean free path of the quasiparticle; therefore, dHvA might miss larger FS pocket and clean samples are required, which has limited its ability to study many of the novel quantum materials. More importantly, the positions and shapes of the FS pockets in momentum space are naturally given by ARPES, while dHvA cannot, as it provides only the volume of the Fermi surface.

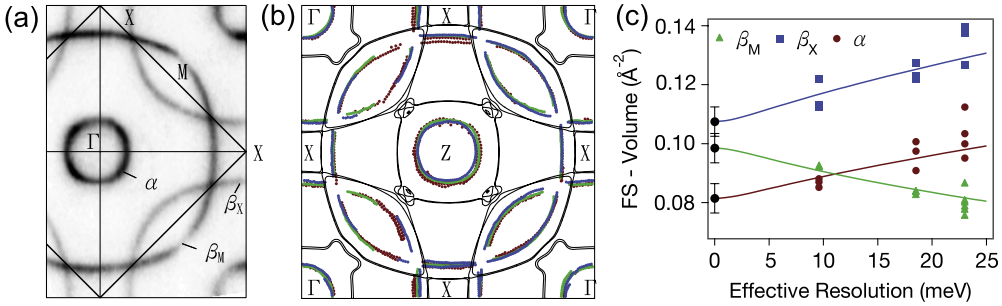


**Figure 4.** (a) Fermi surface mapping of the $Sr_2RhO_4$. (b) The Fermi surface contours determined from the data taken with different resolutions. (c) A summary of the estimated Fermi surface volume for each pocket as a function of energy resolution of the ARPES instrument. Reproduced with permission from [8]. Copyright 2006 by The American Physical Society.

The benchmarking of the ARPES technique is further illustrated in figure 4, which is ARPES measurements on $Sr_2RhO_4$ [8]. This system also has a rather complicated FS, which consists of three different FS pockets, as shown in figure 4(a). This is in contrast to the dHvA measurement on the same materials, in which only one of the Fermi surface pockets, $\beta_M$, can be resolved. To benchmark the precision of ARPES measurement, the size of each FS pocket measured by ARPES is plotted as a function of energy resolution in figures 4(b) and (c), suggesting that the error of FS volume measured by ARPES can be less than 1% at an energy resolution of 10 meV. With this precision, the charge carrier concentration of the $\beta_M$ pocket deduced from ARPES is found to have a good agreement with dHvA measurement. Furthermore, using the effective mass and charge carrier density of each pocket measured by ARPES, the authors estimate the specific heat, which agrees very well with the direct specific heat measurement. This remarkable agreement between the spectroscopy measurement and thermodynamic transport measurement suggests that the ARPES measurement on this system does represent the bulk properties. Moreover, it is the first concrete example that one can start with microscopic information from ARPES data and arrive at a macroscopic property—a feat can only be achieved if we have a microscopic understanding.

In summary, the state-of-the-art ARPES technique is reaching a precision comparable to the bulk-sensitive FS measurement as demonstrated by the two aforementioned examples. This precision and the unique capability of resolving electronic structures in the energy–momentum space makes ARPES an extremely powerful technique to reveal the physics of the novel quantum materials not only qualitatively, but also quantitatively, as will also be further demonstrated in section 2.

## 2. A scientific example of new discovery made by ARPES—energy gap issue of underdoped high-$T_c$ cuprates

The pseudogap state in the underdoped region of the phase diagram is the central intellectual problem in the field of high-$T_c$ superconductivity. Early studies demonstrated that electronic excitations are gapped even at temperatures higher than the superconducting transition temperature $T_c$. This normal state gap is termed a 'pseudogap' because it is not sharply defined, but rather has a broad spectral tail associated with it [9]. The gap is highly anisotropic and most prominent near the Brillouin zone boundary (a.k.a. the antinodal region), reminiscent of its d-wave superconducting state at temperatures below $T_c$ [4]. Because of this similarity and proximity in the phase diagram between the pseudogap state and superconducting state, the relation between the energy gap seen in the pseudogap state and in the superconducting state has been a long-standing question.

The gap measurements made via different experimental probes are, however, seemingly contradictory. On the one hand, as direct probes of electronic states, angle-resolved photoemission spectroscopy (ARPES) on the antinodal region and scanning tunneling microscopy (STM) data have shown that the gap magnitude evolves continuously across $T_c$, suggesting that the pseudogap and superconducting gap are of the same origin [10–13]. The absence of a gap-opening at $T_c$ has been considered as a distinct feature separating the cuprate superconductors from conventional superconductors, in which the pairing gap is the order parameter that dictates the superconducting phase transition. On the other hand, in contrast to earlier ARPES and STM results, a number of gap measurements from other experimental probes reveal a temperature dependent superconducting gap whose magnitude becomes smaller when the temperature approaches $T_c$ and disappears at temperatures above $T_c$. These include the gap measurements from Andreev reflection [14, 15], specific heat [16], intrinsic tunneling [17], and femtosecond spectroscopy [18].

The contradictory results between the single particle probes and others are also seen in the doping dependence of the measured gap magnitude. The gap measured by STM and ARPES near the antinodal region increases when the doped hole concentration in the $CuO_2$ plane reduces (i.e. more underdoped) [19, 20]. Contrarily, the gap measured by penetration depth [21] and Raman spectroscopy [22, 23] suggests that the gap magnitude decreases with more underdoping. In light of these contradictions, a two-gap picture envisioning the pseudogap and superconducting gap being different energy scales has been proposed. This sharply opposes the one-gap picture established from the results of the single particle probes. Clearly, to settle down this issue,

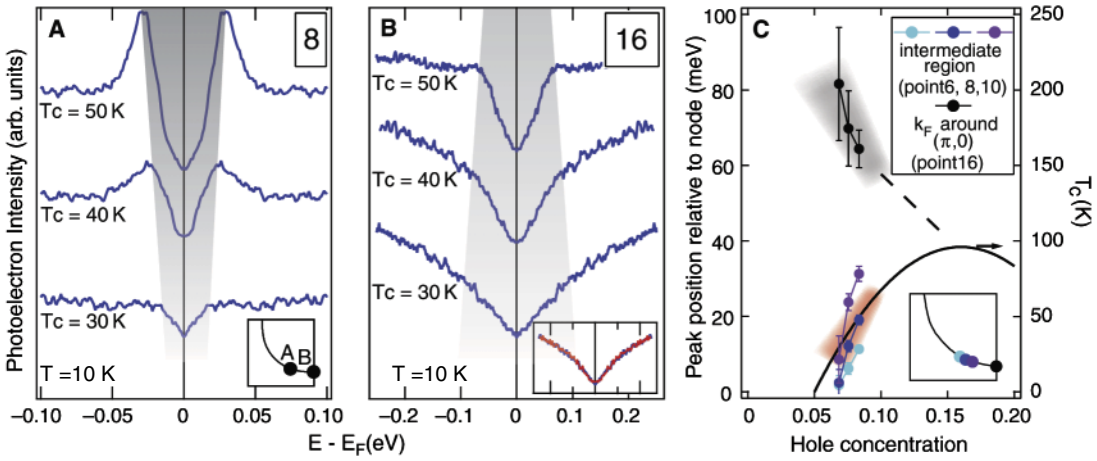


**Figure 5.** (a) Doping dependence of the symmetrized spectra in (a) the intermediate region and (b) the antinodal region. Their corresponding locations on the FS are shown in the inset in (a). The shaded area denotes the region inside the gap determined by the peak positions of the energy distribution curves (EDCs). For the antinodal spectra, the position of the hump, which is determined from the second derivative of the spectra, is used as the peak position. The inset in (b) shows the temperature dependence of the spectra of the $T_c = 30$ K sample taken at 10 K (blue) and 50 K (red) in the antinodal region. (c) A summary of the gap size determined from the symmetrized EDCs at several different locations in the intermediate region (where a peak can be resolved) and the antinodal region. A different trend of the doping dependence is observed. From [25]. Reprinted with permission from AAAS.

it is necessary to understand how to resolve the contradiction between the single particle probes and other measurements.

Most of the earlier gap measurements made by ARPES were focused on the antinodal region; data near the node (diagonal direction of the Brillouin zone) with detailed temperature and doping dependent studies have been scarce until now. This is because the gap near the node is smaller due to the nature of the $d_{x^2-y^2}$ pairing, which is difficult to resolve with the limited resolution and data acquisition efficiency of the earlier ARPES techniques. With the much updated instrumental resolution and data acquisition efficiency of today's state-of-the-art ARPES system, it is now possible to make the gap measurements near the nodal region with much improved resolution and more data points in the momentum space. We have made systematic gap measurements along the entire Fermi surface on samples with different doping levels at different temperatures. We found that, while the behavior of the gap near the antinodal region is consistent with previous ARPES measurements, the gap near the nodal region behaves very differently, shedding a new light on this one-gap versus two-gap issue [24].

We first review a systematic doping dependence study in the heavily underdoped region using Y-doped Bi2212 with $T_c = 30$, 40, and 50 K. The breakthrough of this set of data is that we are able to resolve a quasiparticle peak near the nodal region, which was not resolvable in the previous measurements on samples with a similar doping range. The resolved quasiparticle peak near the nodal region makes possible a gap analysis for these heavily underdoped systems near the nodal region [25]. Surprisingly, as shown in figure 5, the gap associated with this sharp peak region near the node becomes smaller when the system is more underdoped, reflecting the $T_c$ of the samples. We note that that this gap seen near the nodal region is more relevant to the superconductivity since it tracks the $T_c$ of the samples and is associated with a quasiparticle peak. On the contrary, the gap magnitude of the spectrum near the antinodal region for these heavily underdoped samples increases when the system is less doped. This opposite trend of the doping dependence between the nodal region gap and antinodal region gap, together with the very different spectral lineshapes, implies that the pseudogap and superconducting gap are two energy scales. We also note that the region where one can see a quasiparticle peak on the Fermi surface shrinks with more underdoping. This can be interpreted as the expansion of the pseudogap territory from the antinodal region, which suppresses the quasiparticle peaks and shrinks the territory of superconductivity toward the nodal region.

We have also examined this two-gap picture from the aspect of the temperature dependence [26]. We choose to make temperature dependence measurements on the sample near the optimal doping region because the superconducting gap is larger and its temperature dependence near the nodal region can be confidently resolved by our instruments. In contrast to the gap magnitude in the antinodal region, which is known to be rather temperature independent from earlier ARPES measurements [11], the gap near the nodal region appears to vary with temperature significantly. Figure 6 shows the temperature dependence of the gap at a position near the nodal region of the slightly underdoped $Bi_2Sr_2CaCu_2O_{8+\delta}$ cuprate with $T_c = 92$ K. The gap collapses at a temperature very close to $T_c$ with a temperature dependence reminiscent of that predicted by BCS theory (figure 6(b)). With the high resolution of our ARPES measurements, the thermally populated upper Bogoliubov band can also be resolved in raw EDCs for temperatures lower than $T_c$, which moves closer to $E_F$ when the temperature approaches $T_c$ and disappears at temperatures higher than $T_c$ (figure 6(a)). This further confirms that the energy gap observed near the nodal region is clearly related to the superconducting gap, which closes at temperatures close to $T_c$. Figure 6(c) summarizes the temperature dependence of the

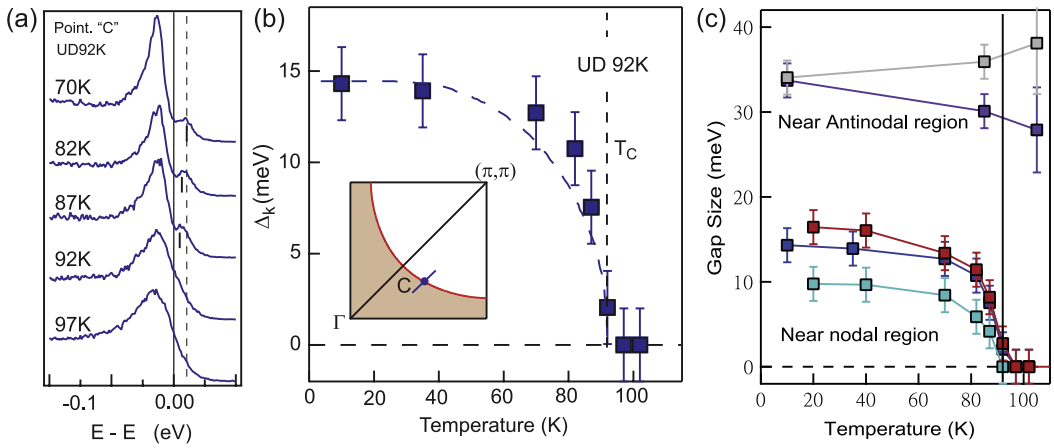


**Figure 6.** Temperature dependence of the gap in slightly underdoped Bi-2212 cuprate. (a) Raw EDCs near the nodal region on the Fermi surface at several different temperatures from below $T_c$ to above $T_c$. The small feature seen above $E_F$ is the upper branch of the Bogoliubov quasiparticle dispersion. (b) The gap size fit from the symmetrized spectrum of (a). The inset indicates the momentum position of the spectrum in the first Brillouin zone. (c) A summary of the temperature dependence of the gap near the nodal and the antinodal region. Reproduced with permission from [26]. Copyright 2007 Nature Publishing Group.

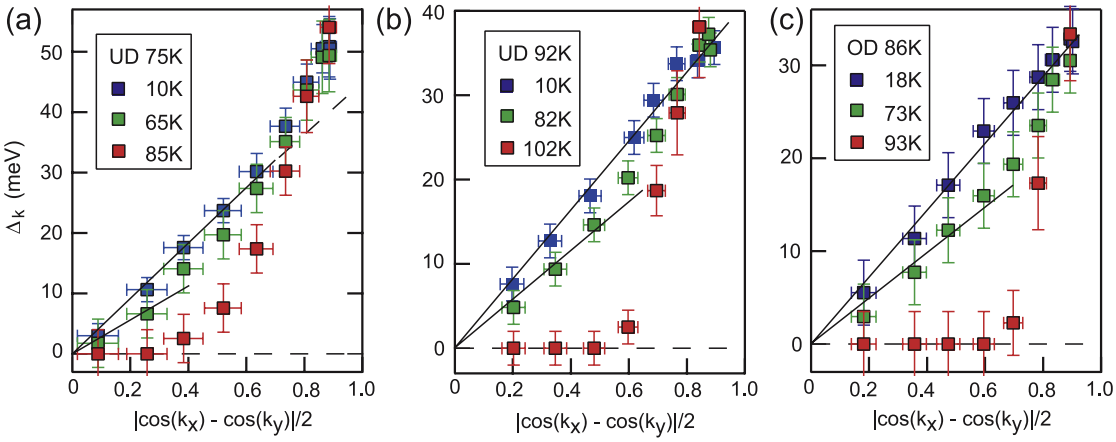


**Figure 7.** Temperature evolution of the gap function of Bi-2212 crystals with three different doping levels with $T_c$ 75 K (UD75K), 92 K (UD92K), and 86 K (OD86K, slightly overdoped sample). Reproduced with permission from [26]. Copyright 2007 Nature Publishing Group.

gap near the antinodal region and nodal region, highlighting the very different temperature dependence behavior. Since it is very un-natural to have one gap behave almost oppositely near the transition temperature, we argue that that the observed temperature dependence is indicative of the existence of two energy gaps in this system [14]. We note that the gap in this intermediate region appears to have a temperature dependence but the gap does not close at $T_c$, indicating a mixture of the nodal and antinodal behavior, which leads to a smooth transition from one to the other.

This different temperature dependence of the gap in different regions of the momentum space results in a very interesting gap function evolution on the Fermi surface. Figure 7 demonstrates the temperature evolution of the gap function for samples with three different doping levels. At the temperature above $T_c$, there exists a gapless region on the Fermi surface that reduces with more underdoping. At temperatures right below $T_c$, this region opens a superconducting gap consistent with a simple d-wave form, $|\cos(k_x) - \cos(k_y)|/2$, while the gap near the antinodal region deviates from this simple d-wave form. Most interestingly, at the lowest temperature, we found that the gap function evolves into a simple d-wave form for the overdoped (OD86K) and slightly underdoped samples (UD92K); however, for the more underdoped sample (UD76K), the gap function does not recover to the simple d-wave form at the lowest temperature we can measure, a reflection of the dominance of the pseudogap. Again, the observed temperature evolution of the gap function is very hard to reconcile within a one-gap picture as the form of the gap function should remain the same once the system enters the superconducting state, at least in the simple mean-field picture. It appears that there is a component of d-wave superconductivity that tries to expand to the entire Fermi surface region (toward the antinodal region) and takes over the territory of the antinodal pseudogap when the system moves 'deeper' into the superconducting state at lower temperature. For the system with sufficient doped hole concentration the d-wave superconducting state manages to take over the entire

Fermi surface at low temperature, while for more underdoped samples the pseudogap effect is too strong for the d-wave superconducting state to fully overcome; therefore, the simple d-wave form of the superconducting gap function can only be extended to a part of the Fermi surface near the nodal region; while the superconducting gap near the antinodal region is mixed with the residual pseudogap component. When the system is further underdoped the quasiparticle peak can be completely suppressed in the antinodal region, as has been discussed as mentioned before in the heavily underdoped region [25].

In summary, our results depict a momentum space picture in which the superconducting gap resides near the nodal region and the pseudogap lives near the antinodal region. The observed temperature and doping dependences have vividly demonstrated the interplay of these two energy gaps. This momentum space picture of the two gaps also provides a natural explanation for resolving the contradictory results between the single particle probe and other experiments, since different experimental probes emphasize different aspects of the electronic structure of the Fermi surface. For example, STM is known to be more sensitive to the antinodal region [19], while the Andreev reflection measurement is directly sensitive to the superconducting condensate—the state near the nodal region. We also note that several recent ARPES measurements from other groups and an increasing number of results from other types of experiments are leading to the same conclusion of a two-gap picture. In any case, we have established a detailed phenomenology of the behavior of the energy gap, which provides further constraints for developing a microscopic theory of the high-$T_c$ superconducting cuprates.

## 3. Summary and outlook

Angle-resolved photoemission spectroscopy has been an extremely powerful tool for mapping the band structure and Fermi surface for solid state samples. We have shown that the precision of the current ARPES measurement is sufficient for performing quantitative analysis comparable to the bulk measurements. In particular, with the improved resolution, precision, and data acquisition efficiency, ARPES as a probe of the many-body effects has also played an increasingly important and valuable role in understanding the physics of novel complex quantum materials. One of the natural future directions for ARPES is to push for an even higher resolution, which will be crucial for the more quantitative analysis on the low energy electronic excitations and their related phenomena. There are also a lot of efforts in progress trying to bring new dimensions into the ARPES technique, such as the spin of the electronic state and the electronic dynamics in the time domain. Many exciting developments of the spin-resolved ARPES and time-resolved ARPES have been made recently using a laser as the light source. In addition, with the further development of the light source, such as the modern accelerator-based free-electron laser (FEL) and the ultra-bright synchrotron light source, it becomes increasingly feasible to develop the so-called 'nano-ARPES', in which ARPES measurement is performed as a nano-scope with a spatial resolution of the order of 10 nm. In any case, in the perceivable future, we envision ARPES will continue evolving and playing an irreplaceable role in the scientific research of complex materials.

## Acknowledgment

This work is supported by DOE Office of Basic Energy Science, Division of Materials Science and Engineering, with contract DE-AC02-76SF00515.

## References

[1] Hertz H 1887 *Ann. Phys., Lpz.* **33** 983
[2] Einstein A 1905 *Ann. Phys., Lpz.* **17** 132
[3] Berglund C N and Spicer W E 1964 *Phys. Rev.* **136** 1030
[4] Damascelli A, Hussain Z and Shen Z 2003 *Rev. Mod. Phys.* **75** 473
[5] Hunfer S 1995 *Photoelectron Spectroscopy* (Berlin: Springer)
[6] Liu G, Wang G, Zhu Y, Zhang H, Zhang G, Wang X, Zhou Y, Zhang W, Liu Haiyun, Zhao L, Meng J, Dong X, Chen C, Xu Z and Zhou X J 2008 *Rev. Sci. Instrum.* **79** 023105
[7] Shen K M, Kikugawa N, Bergemann C, Balicas L, Baumberger F, Meevasana W, Ingle N J C, Maeno Y, Shen Z-X and Mackenzie A P 2007 *Phys. Rev. Lett.* **99** 187001
[8] Baumberger F, Ingle N J C, Meevasana W, Shen K M, Lu D H, Perry R S, Mackenzie A P, Hussain Z, Singh D J and Shen Z-X 2006 *Phys. Rev. Lett.* **96** 246402
[9] Timusk T and Statt B 1999 *Rep. Prog. Phys.* **62** 61
[10] Loeser A G, Shen Z-X, Dessau D S, Marshall D S, Park C H, Fournier P and Kapitulnik A 1996 *Science* **273** 325
[11] Loeser A G, Shen Z-X, Schabel M C, Kim C, Zhang M and Kapitulnik A 1997 *Phys. Rev.* B **56** 14185
[12] Norman M R, Ding H, Randeria M, Campuzano J C, Yokoya T, Takeuchi T, Takahashi T, Mochiku T, Kadowaki K, Guptasarma P and Hinks D G 1998 *Nature* **392** 157
[13] Renner Ch, Revaz B, Genoud J-Y, Kadowaki K and Fischer O 1998 *Phys. Rev. Lett.* **80** 149
[14] Deustcher G 1999 *Nature* **397** 410
[15] Svistunov V M, Tarenkov V Yu, D'Yachenko A I and Hatta E 2000 *JETP Lett.* **71** 289
[16] Loram J W *et al* 1994 *J. Supercond.* **7** 243
[17] Krasnov V M, Yurgens A, Winkler D, Delsing P and Claeson T 2000 *Phys. Rev. Lett.* **84** 5860
[18] Demsar J, Hudej R, Karpinski J, Kabanov V V and Mihailovic D 2001 *Phys. Rev.* B **63** 054519
[19] Fischer O, Kugler M, Maggio-Aprile I, Berthod C and Renner C 2007 *Rev. Mod. Phys.* **79** 353
[20] Harris J M, Loeser A G, Marshall D S, Schabel M C, Shen Z-X, Eckstein J N and Bozovic I 1996 *Phys. Rev.* B **54** R15665
[21] Panagopoulos C and Xiang T 1998 *Phys. Rev. Lett.* **81** 2336
[22] Opel M *et al* 2000 *Phys. Rev.* B **61** 9752
[23] Le Tacon M *et al* 2006 *Nat. Phys.* **2** 537
[24] Millis A J 2006 *Science* **314** 1888
[25] Tanaka K, Lee W S, Lu D H, Fujimori A, Fujii T, Risdiana, Terasaki I, Scalapino D J, Devereaux T P, Hussain Z and Shen Z-X 2006 *Science* **314** 1910
[26] Lee W S, Vishik I M, Tanaka K, Lu D H, Sasagawa T, Nagaosa N, Devereaux T P, Hussain Z and Shen Z-X 2007 *Nature* **450** 81